Detection of Dust Storms Using MODIS Reflective and Emissive Bands

Esam El-ossta, Rami Qahwaji, and Stanley S. Ipson

***Abstract*—Dust storms are one of the natural phenomena, which have increased in frequency in recent years in North Africa, Australia and northern China. Satellite remote sensing is the common method for monitoring dust storms but its use for identifying dust storms over sandy ground is still limited as the two share similar characteristics. In this study, an artificial neural network (ANN) is used to detect dust storm using 46 sets of data acquired between 2001 and 2010 over North Africa by the Moderate Resolution Imaging Spectroradiometer (MODIS) instruments aboard the Terra and Aqua satellites. The ANN uses image data generated from Brightness Temperature Difference (BTD) between bands 23 and 31 and BTD between bands 31 and 32 with three bands 1, 3, and 4, to classify individual pixels on the basis of their multiple-band values. In comparison with the manually detection of dust storms, the ANN approach gave better result than the Thermal Infrared Integrated Dust Index approach for dust storms detection over the Sahara. The trained ANN using data from the Sahara desert gave an accuracy of 0.88 when tested on data from the Gobi desert and managed to detect 90 out of the 96 dust storm events captured worldwide by Terra and Aqua satellites in 2011 that were classified as dusty images on NASA Earth Observatory.**

***Index Terms*—Brightness temperature difference, dust storms, MODIS, normalized difference dust index, satellite remote sensing.**

I. Introduction

DUST storms occur in many areas throughout the world are one of the natural phenomena exacerbated by climate change [1], [2]. Dust storms increase air pollution, which forces people indoors, reduces visibility which delays both road and air traffic and impacts on both urban and rural areas [3]. They cause damage to human health, reduce the temperature, [4] and damage communication facilities [5]. Dust can be transported over very long distances. Sand from Saharan dust storms, for example, caused by a combination of dry conditions and strong winds, can reach as far as the north of Europe and parts of Asia and North America [3]. Interest in monitoring and forecasting dust storms is increasing in order to help governments reduce the negative impact of these storms. At present there are two main methods available for monitoring dust storms: ground based measurements and satellite based remote sensing. The latter is expected to become the primary approach for the detection of dust storms if current problems with obtaining accurate detection under widely varying conditions can be overcome [1] because it has many potential advantages including flexible coverage of wide areas and continuous monitoring. Satellite remote sensing using true-color images or estimates of aerosol optical thickness (AOT) and algorithms such as the deep blue algorithm have limitations for identifying dust storms [6]. Dust storms can be difficult to distinguish from sandy ground and from water clouds in some spectral bands [7] where they have similar characteristics. However, in principle, the severity of dust storms, the areas they affect and changes in intensities can be monitored using appropriate remotely sensed images [4].

Many researchers have proposed methods aiming to distinguish dust storms from clouds, ground and water surfaces using images from instrument such as MERIS [5], TOMS [8], SeaWiFS [9], GOES [10] and MODIS (Terra and Aqua) [1], [2], [4], [5], [11] and those on the satellites NOAA-AVHRR [12], Landsat and GMS [13]. In this study we have concentrated on MODIS (Moderate Resolution Imaging Spectroradiometers) data because it includes 36 spectral bands, which potentially provides more opportunities for developing techniques for the detection of dust storms than the data from other instruments.

Several methods have been presented for the detection of dust storms based on thresholding a quantity calculated from some of the 36 data bands provided by the Moderate Resolution Imaging Spectroradiometer (MODIS) satellite. One based on the so called Normalised Difference Dust Index (NDDI) is proposed to detect dust storms from cloud and non sandy ground [1]. However, it does not give good results over sandy ground such as the Sahara desert because the reflectance of strong dust storms and clouds are similar in band 3. The brightness temperature (BT) of band 31 has been used in NDDI to enhance the detection of dust storm over a bright surface. However, this gives limited results as the BT of thin dust storm and bright surface are similar. Another method [4], used the Brightness Temperature Difference (BTD) between bands 31 and 32 for the detection of dust storms during both day and night in the North West of China in 2006. However the use of BTD with zero thresholds was not enough to prevent some clouds being falsely detected as dust. For this reason the authors used an NDDI technique to remove clouds during the day. However, NDDI is limited for detection dust storm from low cloud as both have the same reflectance at bands 3 and 7. At the same time brightness temperatures greater than 263 K and less than 280 K were used to distinguish dust storms from clouds and land respectively during night time using band 31. This study showed a very effective detection of dust storms.

Neural Networks are widely used in many applications such as data mining and classifying vegetation and other land cover satellite data. Both a Maximum Likelihood classifier (ML) and

Manuscript received July 25, 2012; revised January 10, 2013; accepted February 07, 2013. Date of publication May 02, 2013; date of current version November 21, 2013.

The authors are with the School of Computing Informatics and Media, University of Bradford, Bradford BD7 1DP, U.K.

Color versions of one or more of the figures in this paper are available online at http://ieeexplore.ieee.org.

Digital Object Identifier 10.1109/JSTARS.2013.2248131

a Probabilistic Neural Network (PNN) were used in the development in [14] of an automatic dust storm detection technique trained and tested using a total of 31 dust storm events in the United States. The data used were MODIS multispectral bands from the NASA Terra satellite comprising brightness temperature pixel values from bands 20, 29, 31 and 32. This study found the PNN to be much better than the ML for dust storm detection. The accuracy of detection of dust storms using PNN and ML were 84% and 67% respectively.

The remainder of this paper is organized as follows. Section II briefly reviews MODIS data generally, the data used in this study, analysis using the BTD (b23-b31) method for distinguishing dust storm and cloud from other surfaces, and the use of a Feed-Forward Back Propagation Neural Network for dust storms detection. Section III shows some results of the comparison between the implementation of Feed-Forward Back Propagation Neural Network and the recent Thermal Infrared Integrated Dust Index (TIIDI) [15] technique over the Sahara and Gobi deserts. Section IV concludes this paper and discusses future work.

II. Method and Analysis

The previous technique (TIIDI) using MODIS data for detection of dust storms over other deserts was tested using data from the Sahara desert and was found to perform less effectively than in its original region of application. Thus there is a need to develop systems able to detect dust storms over different geographical regions of the Earth including the Saharan, American, Australian and Gobi deserts. For such a system to be practically useful it should run automatically in real-time.

A. Data

The Data used for the detection and monitoring of Dust Storms in this paper are MODIS level1B data obtained from the imaging Spectroradiometers that are consist on both the Terra and Aqua satellites. Sensors on both satellites provide 36 channels divided into three groups according to resolution. Bands 1 and 2 have 250 m spatial resolution, bands 3 to 7 have 500 m spatial resolution, and bands 8 to 36 have 1 km spatial resolution. Furthermore, bands 1 to 19 and 26 are solar reflectance bands (SRBs) whereas the others are emissive bands. The MODIS instruments provide one MODIS image every five minute from both Terra and Aqua satellites [1], [4], [13].

The MODIS data listed in Table I, selected for investigation in this study, were captured over different areas of the Sahara desert by the Aqua and Terra satellites between 13th May 2005 and 10th June 2010 and between 9th November 2001 and 23rd July 2010 respectively. The individual dates and times are listed in Table I. The times of data used in this study ranged from 05:10 am to 13:55 pm. The first 41 rows of data referred to in Table I have been classified by NASA Earth Observatory (http://earthobservatory.nasa.gov/NaturalHazards/) as containing dust storm images, while the last 9 rows were chosen by authors as they were classified as not containing dust storm images. This classification by the NASA Earth Observatory is done by the visual inspection of the RGB images and the same method has been used to choose dust images in this study.

TABLE I
The Image Data Used in This Study

MODIS Data	Date	Time (GMT)	Satellite
1	2005/05/13	10:35	Aqua
2	2005/07/18	13:40	Aqua
3	2005/07/19	12:45	Aqua
4	2003/02/02	11:20	Aqua
5	2003/02/28	11:55	Aqua
6	2005/03/01	12:20	Aqua
7	2004/05/29	12:00	Aqua
8	2006/02/24	11:30	Aqua
9	2008/06/03	11:45	Aqua
10	2008/06/05	13:15	Aqua
11	2008/06/06	10:40	Aqua
12	2008/06/08	12:05	Aqua
13	2008/06/02	12:40	Aqua
14	2008/06/07	11:20	Aqua
15	2008/06/08	12:00	Aqua
16	2008/06/10	13:30	Aqua
17	2010/04/22	13:25	Aqua
18	2010/05/26	11:35	Aqua
19	2010/05/27	10:40	Aqua
20	2010/05/27	13:55	Aqua
21	2010/06/08	11:00	Aqua
22	2010/06/09	13:25	Aqua
23	2010/06/10	12:30	Aqua
24	2001/11/09	10:45	Terra
25	2002/05/07	10:30	Terra
26	2002/05/08	09:35	Terra
27	2006/02/23	09:15	Terra
28	2006/07/25	08:30	Terra
29	2006/02/25	09:00	Terra
30	2002/07/11	08:00	Terra
31	2008/01/04	11:45	Terra
32	2008/06/04	10:55	Terra
33	2008/06/05	08:20	Terra
34	2006/04/11	05:10	Terra
35	2010/06/08	07:50	Terra
36	2010/06/09	08:35	Terra
37	2010/06/10	10:55	Terra
38	2010/06/10	11:00	Terra
39	2010/07/04	10:05	Terra
40	2010/07/04	10:10	Terra
41	2010/07/24	09:45	Terra
42	2004/03/27	06:50	Aqua
43	2008/06/01	12:00	Aqua
44	2008/06/04	12:30	Aqua
45	2008/01/01	09:35	Terra
46	2008/01/01	11:10	Terra
47	2008/01/02	08:40	Terra
48	2008/01/04	08:25	Terra
49	200801/04	10:05	Terra
50	2008/08/03	09:35	Terra

B. Brightness Temperature Difference (BTD)

The efficiency of emission of thermal radiation compared with a black body is listed in the MODIS UCSB Emissivity Library (http://g.icess.ucsb.edu/modis/EMIS/html/em.html) at different wavelengths for many different surfaces. Inspection of

TABLE II
THE AVERAGE OF THE BRIGHTNESS TEMPERATURE OF WATER, LAND, VEGETATION, DUST STORM AND CLOUD FOR EACH MODIS BAND

Wavelengths	Water	Land	Vegetation	Dust Storm	Cloud
band 32	285.725	310.198	295.567	289.607	270.525
band 31	286.455	309.803	296.075	287.272	271.314
band 23	285.368	310.625	295.683	298.426	276.039
band 22	296.571	321.830	305.5141	309.358	291.410
band 21	376.848	381.070	378.021	378.587	376.258
band 20	291.783	324.742	302.715	317.734	289.271

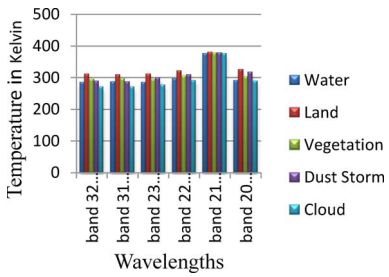

Fig. 1. Brightness temperatures of water, land, vegetation, dust storms and cloud for bands 32, 31, 23, 22, 21, and 20.

the emissivities of sand and sandy soil shows that the emissivity of Sand is higher than the emissivity of Sandy Soil 0.88 and 0.76 respectively at the centre of band 23 (4.06 μm), whereas the emissivities of Sand, Soil, and Sandy Soil in the centre of band 31 (11.02 μm) are similar at 0.96. For this work, the authors assume that the emissivity of sandy soil is lower than sand around 4 μm in MODIS emissivity Library. This suggests that the brightness temperature difference (between 4.06 μm and 11.02 μm) could be useful for distinguishing a dust storm from Sandy Soil. The average brightness temperatures (BT) in a 100×100 pixel window of water, vegetation, cloud, land, snow and dust storm for all MODIS bands, corresponding to surface temperatures, for all 41 images listed in Table I have been calculated and then displayed in charts. A representative sample result for the image identified in row 8 (2006/02/24) of Table I, is shown in Table II and Fig. 1. It was found that BTD (b23-b32) and BTD (b23-b31) can both be used to distinguish between dust storms and cloud and between dust storms and ground surface. However, the BTD (b23-b31) is better, as it is higher than BTD (b23-b32) for dust storms. The BTD between bands 23 and 31 is also useful for detecting dust storm as, for example, the BT of water in band 23 (285 K) is less than the BT of water in band 31 (286 K), also the BT of vegetation in band 23 (295 K) is less than the BT of vegetation in band 31(296 K), while the BT of land in band 23 (310 K) is slightly higher to the BT of land in band 31(309 K), also the BT of cloud in band 23 (276 K) is higher than the BT of band 31 (271 K). While the BT of dust storm in band 23 (298 K) is much higher than the BT of dust storm in band 31 (287 K). For this reason the BTD between band 23 and band 31 will give the values of BTD of water and vegetation less than 0 K, land around 1 K, cloud around 5 K,and dust storm around 11 K. This means that the BTD (b23-b31) could separate dust storms and clouds easily from water, land and sandy land making it more effective than TIIDI.

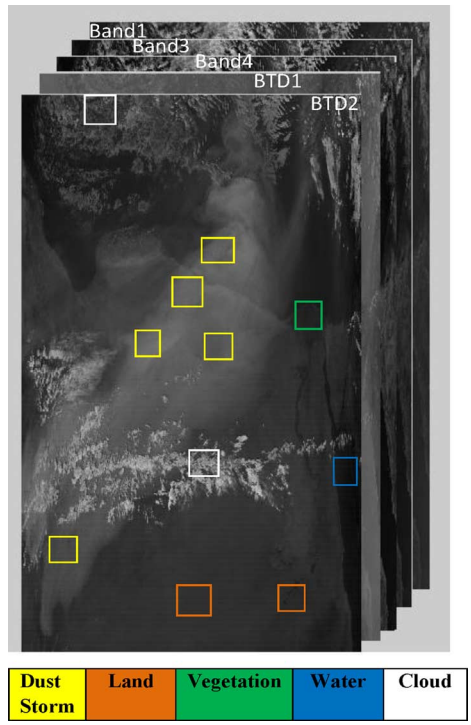

Fig. 2. Illustration of the sampling of the five classes from the three band images and two BTD images from row 8 of Table I.

C. Feed-Forward Back Propagation Neural Network Technique

The threshold method uses fixed value thresholds, but these are different for weak or intense dust storms. For this reason a feed-forward back propagation network based on MATLAB has been used to classify pixels to detect dust storms from weak to intense using data listed in Table I. The feature vector inputs used for the neural network are pixel samples of dust storm, land, cloud, water, and vegetation extracted from multi-spectral MODIS bands 1, 3 and 4, the BTD (b23-b31) used in the previous subsection and the BTD (b31-b32) used in [4] as shown in Fig. 2. MODIS bands 1, 4, and 3 correspond to the components which can be used to construct true-color images showing white for cloud and black for water. Sand and land are both shown similarly as shades of brown and areas of vegetation are green. The true-color images enable cloud, land, water, and vegetation areas to be distinguished while the BTD between bands 23 and 31 is used to distinguish between dust storm and land and the BTD between bands 31 and 32 is used to distinguish between dust storm and cloud. The pixel classification performed here divides the pixels in the remotely sensed images into a binary dust or no-dust classification. There are three steps in this supervised classification:

1) Selection of the training samples for the five different objects of interest from the three bands and the two BTDs, as illustrated in Fig. 2. Windowed regions of the same size (50×50) were cropped from the six object types (dust storm, snow, cloud, land, vegetation and water) in the five images (band 1, band 3, band 4, BTD1 and BTD2). Each window was then converted to one data vector and all data vectors were collected in one matrix ($135{,}000 \times 5$). A

total of 135,000 data components extracted from 24 images were used in this study for training and testing the neural network. Table III shows sample rows of data that were used for training and testing the Neural Network. Rows 1–3 correspond to the pixels from the "dust" class and rows 4–8 correspond to pixels from the "no-dust" class chosen from pixels representing Cloud, Vegetation, Land, Water and Snow respectively.

2) The pixel data were divided into two sets with 60% of pixels data used for training the neural network and the remaining 40% used for testing.
3) The performance of the neural network was evaluated using manual detection of dust storms from the true-color images because no other source of ground truth date is available. This method of generating ground truth data was also used by some of the authors mentioned in Section I. Eight performance metrics were used in this study: True positive rate (TPR), False positive rate (FPR), True negative rate (TNR), False negative rate (FNR), Accuracy (ACC), Positive predictive value (PPV), Negative predictive value (NPV) and False discovery rate (FDR). These are defined as follows [16].

$$TPR = \frac{\sum TP}{\sum (TP + FN)} \tag{1}$$

$$FPR = \frac{\sum FP}{\sum (FP + TN)} \tag{2}$$

$$TNR = \frac{\sum TN}{\sum (TN + FP)} \tag{3}$$

$$FNR = \frac{\sum FN}{\sum (FN + TP)} \tag{4}$$

$$ACC = \frac{\sum (TP + TN)}{\sum (TP + FP + TN + FN)} \tag{5}$$

$$PPV = \frac{\sum TP}{\sum (TP + FP)} \tag{6}$$

$$NPV = \frac{\sum TN}{\sum (TN + FN)} \tag{7}$$

$$FDR = \frac{\sum FP}{\sum (FP + TP)}. \tag{8}$$

Here ΣTP (true positive) corresponds to the number of dust pixels detected as dust. ΣTN (true negative) corresponds to the number of non-dust pixels and detected as non-dust. ΣFP (false positive) corresponds to the number of non-dust pixels detected as dust. ΣFN (false negative) corresponds to the number of dust pixels detected as non-dust. Sample results are shown in Table IV.

III. Results

The Neural Network based approach was applied to MODIS data from the Terra and Aqua satellites acquired over Africa and listed in Table I. The performance of this approach was assessed using several standard measures, with ground truth data as shown in Table IV. The Neural Network based approach was compared with the TIIDI technique (applied by the authors) for the detection of dust storms over bright surfaces, and was found to be much better for detecting dust storms than in the latter as shown in Table IV, the TPR values for both methods are the same. However, the FPR from ANN is less than from TIIDI and that means less cloud and sandy land were detected as dust storm. Also the ACC from ANN is higher than from TIIDI. Furthermore, the FDR from ANN is less than from TIIDI, which means that false detective values in ANN are fewer than from TIIDI. Also, the ANN method was found to give better results for FPR, ACC and FDR than the TIIDI method for Gobi desert data as shown in Table V and in Fig. 4. Both ANN and TIIDI methods can distinguish dust storms from cloud, water and vegetation surfaces. However, TIIDI is poorer at distinguishing between dust storms and sandy land.

TABLE III
A Small Sample of the Data Used for Training and Testing the Neural Network. Numbers in Columns 1 to 3 are Reflectance Values and in Columns 4 and 5 are BTD Values. the Class Values 0.9 Correspond to Dust Storm and 0.1 Correspond to Regions Containing No Dust Storm, Which Could be Cloud, Vegetation, Land, Water or Snow

NO	Band1	Band3	Band4	BTD1	BTD2	Class
1	0.376	0.224	0.293	10.891	-2.222	0.900
2	0.369	0.221	0.288	11.403	-2.237	0.900
3	0.352	0.214	0.276	10.914	-2.190	0.900
4	0.259	0.181	0.202	4.397	-0.144	0.100
5	0.079	0.127	0.108	0.164	0.469	0.100
6	0.318	0.140	0.195	2.414	-0.264	0.100
7	0.057	0.121	0.075	1.141	0.370	0.100
8	0.125	0.136	0.121	-0.305	-0.070	0.100

TABLE IV
Comparison Between Neural Network (ANN) Method and TIIDI Technique Applied on Sahara Desert Using Eight Measures: True Positive Rate (TPR), False Positive Rate (FPR), True Negative Rate (TNR), False Negative Rate (FNR), Accuracy (ACC), Positive Predictive Value (PPV), Negative Predictive Value (NPV) and False Detective Rate

	ANN	TIIDI
TPR	0.801165	0.807954
FPR	0.028556	0.282141
TNR	0.971444	0.717859
FNR	0.198835	0.192046
ACC	0.945962	0.735488
PPV	0.812211	0.293153
NPV	0.963215	0.962527
FDR	0.187789	0.706847

A. Sahara Desert

After training, the neural network was able to detect dust storms over parts of northern Africa, using the images listed in Table I, with accuracies (as defined in (5)) ranging from 0.832 to 0.999 and an average accuracy of 0.937. Table IV shows the detailed numerical results and corresponding averages for TPR, FPR, TNR, FNR, ACC, PPV, NPV as well as FDR. It can be seen in Table IV and Fig. 3 that the neural network approach provides better performance compared to the TIIDI approach using BTD between bands 23 and 31 for all cases, as indicated by the FPR, ACC, PPV and FDR values. The lower FPR value indicates that the system reduced the numbers of dust pixels that

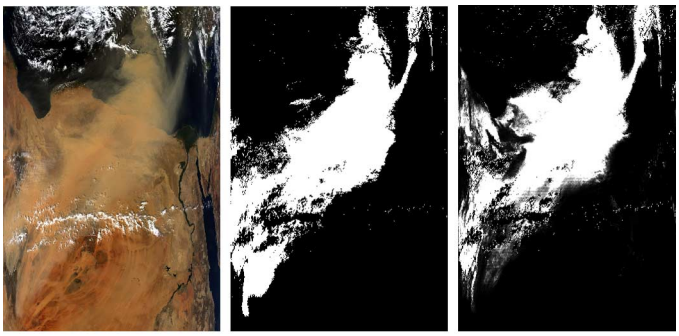

(a) (b) (c)

Fig. 3. (A) shows the dust storm over Sahara and Mediterranean Sea for image row 8 in Table I, using the three true-color bands and (B) is the result of dust storm detection using the trained Neural Network. (C) is the corresponding result from of the technique used in [15].

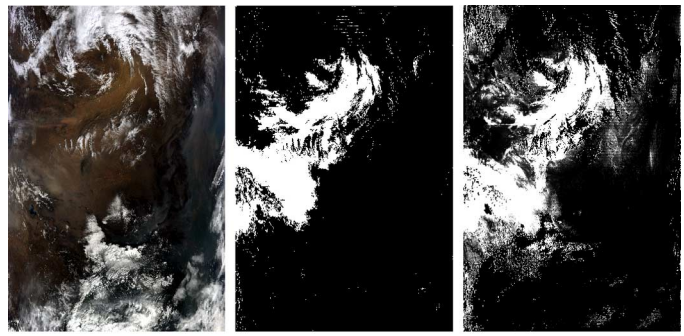

(a) (b) (c)

Fig. 4. 10 (A) is the true-color Aqua image of a dust storm over north China used in TIIDI method; (B) is the result of dust storm detection using the neural network; (C) is the corresponding result from of the TIIDI technique used in [15].

TABLE V
COMPARISON BETWEEN NEURAL NETWORK (NN) METHOD AND TIIDI TECHNIQUE APPLIED ON GOBI DESERT USING EIGHT MEASURES: TRUE POSITIVE RATE (TPR), FALSE POSITIVE RATE (FPR), TRUE NEGATIVE RATE (TNR), FALSE NEGATIVE RATE (FNR), ACCURACY (ACC), POSITIVE PREDICTIVE VALUE (PPV) , NEGATIVE PREDICTIVE VALUE (NPV) AND FALSE DETECTIVE RATE

	ANN	TIIDI
TPR	0.86335	0.87194
FPR	0.11956	0.32790
TNR	0.88044	0.67210
FNR	0.13664	0.12806
ACC	0.88038	0.68541
PPV	0.33634	0.15911
NPV	0.98792	0.98543
FDR	0.66365	0.84089

were falsely detected as dust storm. The effectiveness of the ANN approach for reducing the amount of cloud and shadow falsely included with detected dust storm compared with the TIIDI approach for the data is illustrated in Fig. 3. The neural network also detects more of the dust storm over water than the TIIDI method.

B. Gobi Desert

The neural network system trained only on the Saharan data was further tested in the detection of dust storms over the Gobi desert and Taklimakan desert. It was found that these too can be detected, but with a somewhat less effective performance than for the detection of dust storms over the Sahara desert, as summarised in Table V for comparison with Table IV. However, these results are better than in previous work, as illustrated in Fig. 4, in which the two results can be compared.

This trained ANN has been further tested using all the dust storm events that occurred worldwide in 2011 according to the Earth Observatory (http://earthobservatory.nasa.gov/NaturalHazards/). Of the 96 dust storm events, only 6 were not detected by the ANN and all of these represent very weak dust storms.

IV. CONCLUSIONS

In this study we demonstrate the application of a new approach for the detection of dust storms over northern Africa, where the dust storms and land have similar characteristics, using MODIS data from Terra and Aqua satellites. The Artificial Neural Network binary classifier approach uses the reflectance data of bands 1, 2 and 3, and Brightness Temperature Differences between bands 23 and 31 and between bands 31 and 32. This approach gives better results than previous work (TIIDI), as quantified by TPR, FPR, ACC and FDR values in both Tables IV and V, since dust storms can clearly be separated from the high cloud, land, water, vegetation, snow, low cloud, and cloud shadow. Furthermore, this ANN trained on Saharan data can also detect dust storms over China. This new automated method of using ANN for detecting dust storms could be used for monitoring dust storms in order to help governments reduce the negative impact of these storms. Previous works have limitation on detecting dust storms over sandy land and they do not seem to perform well over different ground surfaces. We believe our ANN-based method increases the quality of detection of dust storms. Furthermore, the ANN-based method can detect dust storms over different ground surfaces. We found that the average of correct classification index (ACC) for this method is about 0.94 and 0.88 over the Sahara and Gobi deserts respectively. However, this method has limitation for detecting dust storms over water and can not be used during night time. Attempting to improve the classification accuracy further, future work will extend the Neural Network method by considering groups of pixels rather than individual pixels and add additional output classes including land, dust storm, vegetation, water, snow and cloud instead of the binary classification dust or no-dust. Also it will aim to include tracking of dust storms using MODIS data.

ACKNOWLEDGMENT

The authors would like to thank Mr. J. Kuyper (MODIS Level 1 Lead, Science Data Support Team), who provided helpful information and many constructive suggestions and comments.

REFERENCES

[1] J. J. Qu *et al.*, "Asian dust storm monitoring combining Terra and Aqua MODIS SRB measurements," *IEEE Geosci. Remote Sens. Lett.*, vol. 3, pp. 484–486, 2006.

[2] S.-C. Liu *et al.*, "Detection of dust storms by using daytime and nighttime multi-spectral MODIS images," in *Proc. IEEE Int. Conf. Geoscience and Remote Sensing Symp., IGARSS*, 2006, pp. 294–296.

[3] H. El-Askary *et al.*, "Introducing new approaches for dust storms detection using remote sensing technology," in *Proc. IEEE Int. Conf. Geoscience and Remote Sensing Symp., IGARSS*, 2003, vol. 4, pp. 2439–2441.
[4] D. Mei *et al.*, "A dust storm process dynamic monitoring wiith multi-temporal MODIS data," *Int. Archives of the Photogrammetry, Remote Sensing and Spatial Inform. Sciences*, vol. XXXVII, pt. B7, pp. 965–970, 2008.
[5] W. Kaiping *et al.*, "Detection of sand and dust storms from MERIS image using FE-Otsu alogrithm," in *Proc. 2nd Int. Conf. Bioinformatics and Biomedical Eng., ICBBE*, 2008, pp. 3852–3855.
[6] H. Barnum *et al.*, "Forecasting dust storms using the CARMA-dust model and MM5 weather data," *Environmental Modelling & Software*, vol. 19, pp. 129–140, 2004.
[7] M. Rijkenberg and E. Achterberg, *Chasing Saharan Dust Storms*. Swindon, U.K.: Natural Environment Research Council, 2006.
[8] X. Hao and J. J. Qu, "Saharan dust storm detection using moderate resolution imaging spectroradiometer thermal infrared bands," *J. Appl. Remote Sens.*, vol. 1, pp. 013510–9, 2007.
[9] N. Steven, D. Miller, C. A. Monterey, and T. F. Lee, "Desert dust storms as detected by Meteosat and SeaWiFS multispectral imagery," in *11th Conf. Satellite Meteorology and Oceanography*, 2001.
[10] J. Pat *et al.*, "Monitoring dust storms and mapping landscape vulnerability to wind erosion using satellite and ground-based digital images," *Using Geospatial Technologies to Understand Dryland Dynamics*, pp. 1092–5481, 2002.
[11] T. Han *et al.*, "Automatic detection of dust storm in the northwest of China using decision tree classifier based on MODIS visible bands data," in *Proc. IEEE Int. Conf. Geoscience and Remote Sensing Symp., IGARSS*, 2005, pp. 3603–3606.
[12] S. Janugani *et al.*, "Directional analysis and filtering for dust storm detection in NOAA-AVHRR imagery," in *Proc. SPIE*, 2009, pp. 73341G–73341G-12.
[13] N. Iino *et al.*, "Detection of Asian dust aerosols using meteorological satellite data and suspended particulate matter concentrations," *Atmospheric Environment*, vol. 38, pp. 6999–7008, 2004.
[14] P. Rivas-Perea *et al.*, "Automatic dust storm detection based on supervised classification of multispectral data," in *Soft Computing for Recognition Based on Biometrics*, P. Melin, Ed. *et al.* Berlin Heidelberg: Springer, 2010, vol. 312, pp. 443–454.
[15] L. Yang and L. Ronggao, "A thermal index from modis data for dust detection," in *Proc. IEEE Int. Conf. Geoscience and Remote Sensing Symp., IGARSS*, 2011, pp. 3783–3786.
[16] T. Fawcett, "An introduction to ROC analysis," *Pattern Recognition Lett.*, vol. 27, pp. 861–874, 2006.

Esam Elossta was born in Ghryan, Libya, in 1977. He received the B.Sc. degree in computer programming from the Higher Institute of Professions Comprehensive, Ghryan, Libya, in 2000, and the M.Sc. degree in computing from the University of Bradford, U.K., in 2007. Since October 2008, he has been working towards the Ph.D. degree in dust storm detection using satellite images.

From 2001 to 2005, he was a Research Assistant with the Libyan Centre for Remote Sensing and Space Science, Tripoli, Libya. He is the author of one conference paper for dust storm detection. His research interests include 2D Image processing and machine learning and remote sensing.

Rami Qahwaji was born in Kuwait in 1972. He received the B.Sc. degree in electrical engineering in 1994 and the M.Sc. degree in control and computer engineering in 1997 from the University of Mustansiriyah, Bagdad, Iraq, and the Ph.D. degree in computer vision system in 2002 from the University of Bradford, Bradford, U.K.

He is currently Professor of Visual Computing. His research interests include: 2D/3D image processing, machine learning and the design of machine vision systems with proven track record in the fields of solar imaging, remote sensing, medical imaging, data visualization and applied data mining working with various medical and industrial collaborators. His research has been funded by leading funding agencies in the U.K. and Europe. He has over 120 refereed publications and has supervised 18 completed Ph.D. projects. He acted as external examiner/reviewer for over 10 U.K. and international universities. He is also a reviewer for many journals and is heavily involved in conferences organization.

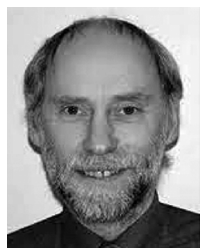

Stanley S. Ipson was born in the U.K. He received the B.Sc. degree in applied physics and the Ph.D. degree in theoretical nuclear physics in 1975 from the University of Bradford, Bradford, U.K.

Since 1975 he is a Senior Lecturer at the University of Bradford. His main research focus is imaging and includes amongst other fields extracting 3D information from uncalibrated images, remote sensing, deblurring infrared and millimetre wave images; optical control of industrial machinery; video camera surveillance; texture analysis; digital image watermarking; and a variety of pattern recognition applications. He has been principal investigator for a number of imaging-related projects, receiving funding from EPSRC, DERA, EU FP7, plus several industrial research contracts. He has supervised around 24 completed Ph.D. projects and held two patents. His publications include invited chapters for four books, around 70 refereed journal papers and conference proceedings and around 35 conference presentations.